Advances in Computational Mathematics (2024) 50:16
https://doi.org/10.1007/s10444-024-10113-y

Conditioning and spectral properties of isogeometric collocation matrices for acoustic wave problems

Elena Zampieri[1] · **Luca F. Pavarino**[2]

Received: 29 December 2022 / Accepted: 15 February 2024 / Published online: 4 March 2024

Abstract

The conditioning and spectral properties of the mass and stiffness matrices for acoustic wave problems are here investigated when isogeometric analysis (IGA) collocation methods in space and Newmark methods in time are employed. Theoretical estimates and extensive numerical results are reported for the eigenvalues and condition numbers of the acoustic mass and stiffness matrices in the reference square domain with Dirichlet, Neumann, and absorbing boundary conditions. This study focuses in particular on the spectral dependence on the polynomial degree p, mesh size h, regularity k, of the IGA discretization and on the time step size Δt and parameter β of the Newmark method. Results on the sparsity of the matrices and the eigenvalue distribution with respect to the number of degrees of freedom d.o.f. and the number of nonzero entries nz are also reported. The results show that the spectral properties of the IGA collocation matrices are comparable with the available spectral estimates for IGA Galerkin matrices associated with the Poisson problem with Dirichlet boundary conditions, and in some cases, the IGA collocation results are better than the corresponding IGA Galerkin estimates, in particular for increasing p and maximal regularity $k = p - 1$.

Keywords Acoustic waves · Absorbing boundary conditions · Isogeometric analysis · Collocation · Newmark method · Condition number · Spectral properties

Mathematics Subject Classification (2010) 65M06 · 65M70 · 65M12

Communicated by: Lourenco Beirao da Veiga

✉ Elena Zampieri
elena.zampieri@unimi.it

Luca F. Pavarino
luca.pavarino@unipv.it

[1] Department of Mathematics, Università di Milano, Via Saldini 50, 20133 Milano, Italy

[2] Department of Mathematics, Università di Pavia, Via Ferrata 5, 27100 Pavia, Italy

1 Introduction

Isogeometric analysis (IGA) has generated a large amount of work since its introduction in Hughes et al. [19], with important results in various fields involving the numerical solution of partial differential equations. The advantages of the IGA approach in many problems and applications have been shown in several studies, see, e.g., Bazilevs et al. [3], Auricchio et al. [1], Cottrell et al. [6], Beirão da Veiga et al. [4], and the references therein. IGA basis functions associated with B-splines and non-uniform rational B-splines (NURBS) are employed to discretize both the problem domain, as in computer-aided design (CAD) systems, and the solution space of the differential problem. In this way, IGA yields an accurate representation of the problem geometry and at the same time a high-order method with respect to standard p- and hp- refinements, where p is the polynomial degree of the IGA basis functions and h is the mesh size. IGA also affords an additional k-refinement, where $k \leq p-1$ is the global regularity of the IGA basis functions, providing highly regular numerical solutions and better accuracy than in the case of classical FEM p-refinement.

While initially IGA studies have been carried out using standard Galerkin approaches, more recently IGA collocation variants have been investigated, with the aim of dealing with sparser mass and stiffness matrices than those arising from IGA Galerkin techniques. IGA collocation has also the additional advantage of reducing the global computational cost, since collocation matrices require only one function evaluation per collocation point, independently of p; see Auricchio et al. [2], Cottrell et al. [7], Dedé et al. [8], Evans et al. [13], Hughes et al. [20], Komatitsch et al. [23], Kruse et al. [25], Zhu et al. [38].

In our previous work [36], we have considered IGA Galerkin and explicit Newmark approximations of the acoustic wave equation with absorbing boundary conditions, whereas in [37], we have extended the study to IGA collocation and implicit Newmark schemes. We presented several numerical results showing the convergence and stability properties of these schemes, and we have reported also a detailed comparison between IGA Galerkin and IGA Collocation with respect to the space and time discretization parameters, CPU time, sparsity of matrices and degrees of freedom. Since both the IGA Galerkin and collocation mass matrices become denser for increasing p and k, the main difference between explicit and implicit IGA Newmark schemes is related to the stability bounds for the time step size, rather than to the cost of the solution of the linear systems at each temporal instant. The theoretical analysis in [36] is confined to the stability properties of the IGA Galerkin Newmark method and additionally, it is only partially based on proven results. In fact, there is still a lack of theoretical spectral bounds for IGA matrices in the literature, and most of the known estimates regarding eigenvalues and conditioning of the IGA mass and stiffness matrices are conjectures. For these reasons, a detailed experimental analysis is of interest in the framework of wave propagation problems in order to explore the gaps of the theoretical analysis and to investigate efficient solution of the linear system at each time step of the time-advancing scheme, possibly involving preconditioning techniques.

Among other relevant works, Gervasio et al. [16] presented an extensive numerical comparison between the Spectral Element Method and NURBS-based IGA Galerkin when applied to the Poisson problem, analyzing the convergence, computational costs, and conditioning with respect to h and p, for minimal ($k = 0$) and maximal ($k = p-1$) regularity of the IGA basis functions. In [24], Loli et al. have studied the condition number of IGA Galerkin mass matrices and have proposed efficient preconditioners for the related linear systems, focusing in particular on k-refinement. In Evans et al. [13], the spectral properties of a semi-discrete predictor-multicorrector method have been investigated for the case of a 1D pure Dirichlet IGA problem.

In this paper, we consider the approximation of acoustic wave problems with absorbing boundary conditions based on IGA collocation at Greville points in space and Newmark advancing schemes in time, both explicit and implicit. We observe that the implementation of absorbing boundary conditions is mathematically equivalent to the more common Robin boundary conditions, as it involves a linear combination of the values of the function and of its normal derivative at the collocation points on the domain boundary. Differently from our previous works [36] and [37], where we focused on the convergence and stability properties of IGA Galerkin and collocation methods, in this paper, we focus instead on the spectral properties of the mass and stiffness matrices for acoustic wave problems discretized with IGA collocation in space and Newmark methods in time. We present a numerical study of the behavior of the eigenvalues and condition numbers of the mass and stiffness matrices in the reference square domain with Dirichlet, Neumann, and absorbing boundary conditions, varying the polynomial degree p, mesh size h, regularity k, time step size Δt and parameter β of the Newmark method. We also report some results on the sparsity of the matrices and the eigenvalue distribution with respect to the degrees of freedom d.o.f. and the number of nonzero entries nz. In order to provide a simple basis of comparison, we recall some bounds and estimates that are available for IGA Galerkin matrices associated to the Poisson problem with Dirichlet boundary conditions, see Gahalaut and Tomar [14], Garoni et al. [15] and Gervasio et al. [16]. Our results show that the same estimates hold for the condition numbers of the IGA collocation matrices considered in this paper, and in some cases, the IGA collocation results are better than the corresponding IGA Galerkin estimates, in particular for increasing p and maximal regularity $k = p - 1$.

The rest of the paper is organized as follows. The acoustic wave model problem and its mathematical analysis are introduced in Section 2, and its approximation by IGA collocation in space and Newmark methods in time in Section 3. In Section 4, we give a brief overview of eigenvalue and condition number estimates for the IGA Galerkin approximation of the Poisson problem. Finally, in Section 5, we present several numerical tests on the behavior of eigenvalues and condition numbers of IGA collocation mass and stiffness matrices with different types of boundary conditions, varying all the discretization parameters, and compare the results with the ones reported for the IGA Galerkin case.

2 The model problem and mathematical analysis

We consider the two-dimensional acoustic wave problem (see, e.g., Junger and Feit [22] and Ihlenburg [21]):

$$\frac{\partial^2 u}{\partial t^2}(\mathbf{x}, t) - c_0 \Delta u(\mathbf{x}, t) = f(\mathbf{x}, t) \quad \text{in } \Omega \times (0, T), \tag{1}$$

where u is the unknown acoustic pressure, c_0 is the acoustic wave propagation velocity, f is the source term. Here, $\Omega = [0, 1] \times [0, 1]$ is the reference square in the plane, $\partial\Omega$ is its boundary and $(0, T)$ is the temporal interval, with T real and positive. Any point of Ω is denoted by $\mathbf{x}$ and t represents the time. The wave equation is subject to initial conditions:

$$u(\mathbf{x}, 0) = \mathcal{U}_0(\mathbf{x}), \qquad \frac{\partial u}{\partial t}(\mathbf{x}, 0) = \mathcal{W}_0(\mathbf{x}) \qquad \text{in } \Omega, \tag{2}$$

where $\mathcal{U}_0$ and $\mathcal{W}_0$ are the initial pressure and velocity, respectively.
Standard Dirichlet or Neumann boundary conditions can be prescribed on $\partial\Omega$:

$$u(\mathbf{x}, t) = \Phi(\mathbf{x}, t) \quad \text{on } \Gamma_D \times (0, T), \qquad \frac{\partial u}{\partial \mathbf{n}}(\mathbf{x}, t) = \Psi(\mathbf{x}, t) \quad \text{on } \Gamma_N \times (0, T). \tag{3}$$

where Φ and Ψ are the prescribed pressure and velocity on Γ_D and Γ_N, respectively, and $\mathbf{n}$ is the outward boundary normal unit vector. We recall that when $\Psi = 0$ the homogeneous Neumann condition represents a free surface resulting in full reflection, whereas the case $\Psi \neq 0$ occurs when a source is located at the portion of the boundary Γ_N. Nevertheless, Dirichlet conditions are less common in acoustic wave problems, since the physical solution is rarely known at some part of the boundary. Other common boundary conditions in the simulation of wave propagation through an unbounded domain are the so called absorbing boundary conditions (ABCs for brevity), involving a truncation of the infinite original domain. On artificial boundaries of the novel finite domain, suitable boundary conditions are then enforced with the aim to get rid of spurious wave reflections as much as possible. Since full absorbing boundary conditions are non-local neither in space nor in time, and consequently not appropriate for implementation, several ABCs have been introduced in the literature in order to make the boundary transparent to outgoing and opaque to ingoing waves (see, e.g., Clayton and Engquist [5] and Engquist and Majda [12]). Here, we study the most common first-order ABCs based on first spatial and temporal partial derivatives only introduced in Mur [27]:

$$\frac{1}{\sqrt{c_0}} \frac{\partial u}{\partial t}(\mathbf{x}, t) + \frac{\partial u}{\partial \mathbf{n}}(\mathbf{x}, t) = 0 \qquad \text{on } \Gamma_{AB} \times (0, T). \tag{4}$$

Here Γ_{AB} is the artificial boundary where ABCs are enforced. Thus, in the most general case, $\partial\Omega = \Gamma_D \cup \Gamma_N \cup \Gamma_{AB}$, where Γ_D, Γ_N and Γ_{AB} are disjoint sets.

The proof of the uniqueness of the solution and stability of the continuous acoustic wave problem (1)-(4) can be performed following the analogous analysis of elasto-dynamics linear problems (see Quarteroni et al. [29]).
Higher-order ABCs could be considered involving also derivatives of order greater than one in space and time, and derivatives in the tangential direction (see, e.g., Givoli [17]).

3 Approximation of the wave problem by isogeometric collocation and Newmark methods

We now discretize the strong form of the acoustic wave problem (1)-(4) by using the collocation variant of isogeometric analysis in space and Newmark schemes in time.

3.1 Isogeometric analysis and collocation methods

Consider a knot vector of non-decreasing real numbers on the reference interval

$$\{\xi_1 = 0, ..., \xi_{\nu+p+1} = 1\}. \tag{5}$$

We assume open knot vectors, i.e., the boundary knots have multiplicity $p+1$ with $\xi_1 = \xi_2 = \cdots = \xi_{p+1}$ and, similarly, $\xi_{\nu+1} = \xi_{\nu+2} = \cdots = \xi_{\nu+p+1}$. With this knot vector, we associate univariate B-spline basis functions N_i^p, where the integers p and ν are the polynomial degree of the B-spline, and the number of basis functions and control points, respectively. B-splines functions are built recursively starting from piecewise constant functions when $p = 0$, obtaining B-splines with support (ξ_i, ξ_{i+p+1}), $i = 1, 2, ..., \nu$ (see, e.g., Schumaker [31]). It is known that B-spline basis functions are C^{p-1}-continuous if internal nodes are not repeated, whereas they are C^k-continuous with $k = p - \alpha$ if the associated knot is repeated α times. When $\alpha = p$, the basis function is C^0-continuous and interpolates the control point at that location where the knot has multiplicity $\alpha = p$. We will assume that the maximum knot multiplicity is p, which ensures the global continuity of our basis functions.
Multi-dimensional B-spline functions are then constructed by tensor products starting from the one-dimensional spline space

$$\widehat{\mathcal{S}}_h = \text{span}\{N_i^p(\xi), i = 1, \ldots, \nu\}. \tag{6}$$

For simplicity of exposition, we examine here the case of a two-dimensional domain, and B-spline of same degree p in each direction. The case of higher-dimensional case and different degrees is analogous. We introduce the two-dimensional parametric space $\widehat{\Omega} := (0, 1) \times (0, 1)$ with a knot vector (5) in each direction, and a net of ν^2 control points $\mathbf{C}_{i,j}$, $i, j = 1, ..., \nu$. The bi-variate spline basis on $\widehat{\Omega}$ is then $B_{i,j}^p(\xi, \eta) = N_i^p(\xi) N_j^p(\eta)$. Similarly, the mesh of rectangular elements in the parametric space is generated in a natural way by the Cartesian product of two-knot vectors $\{\xi_1 = 0, ..., \xi_{\nu+p+1} = 1\}$. Then, $\widehat{\mathcal{S}}_h = \text{span}\{B_{i,j}^p(\xi, \eta),\ i, j = 1, \ldots, \nu\}$, is the

bi-variate spline space analogous to (6). We recall that a rational B-spline in $\mathbb{R}^d$ is the projection onto d-dimensional physical space of a polynomial B-spline defined in $(d+1)$-dimensional homogeneous coordinate space and all conic sections in physical space can be obtained exactly: see Rogers [30] and references therein for a discussion of these space projections. We denote a one-dimensional NURBS basis function of degree p as

$$R_i^p(\xi) = \frac{N_i^p(\xi)\omega_i}{\sum_{\hat{i}=1}^{\nu} N_{\hat{i}}^p(\xi)\omega_{\hat{i}}} = \frac{N_i^p(\xi)\omega_i}{w(\xi)}, \tag{7}$$

with $w(\xi) = \sum_{\hat{i}=1}^{\nu} N_{\hat{i}}^p(\xi)\omega_{\hat{i}} \in \widehat{\mathcal{S}}_h$ a weight function. Analogously to the construction of B-splines, NURBS basis functions on the two-dimensional parametric space $\widehat{\Omega}$ are obtained from the bi-variate spline basis as

$$R_{i,j}^p(\xi,\eta) = \frac{B_{i,j}^p(\xi,\eta)\omega_{i,j}}{\sum_{\hat{i},\hat{j}=1}^{\nu} B_{\hat{i},\hat{j}}^p(\xi,\eta)\omega_{\hat{i},\hat{j}}} = \frac{B_{i,j}^p(\xi,\eta)\omega_{i,j}}{w(\xi,\eta)}, \tag{8}$$

where $\omega_{i,j} \in \mathbb{R}$, and the denominator is the two-dimensional weight function commonly denoted by $w(\xi,\eta)$. NURBS basis functions have the same continuity and support of B-splines, and NURBS spaces are the span of the basis functions (8). Let us consider a *single-patch* domain Ω as a NURBS region associated with the net $\mathbf{C}_{i,j}$. We introduce the geometrical map $\mathbf{F} : \widehat{\Omega} \to \Omega$ defined by

$$\mathbf{F}(\xi,\eta) = \sum_{i,j=1}^{\nu} R_{i,j}^p(\xi,\eta)\mathbf{C}_{i,j}. \tag{9}$$

In the isogeometric paradigm, the space of NURBS scalar fields on the domain Ω is defined as the span of the *push-forward* of the basis functions (8)

$$\mathcal{N}_h := \text{span}\{R_{i,j}^p \circ \mathbf{F}^{-1}, \text{ with } i, j = 1, \ldots, \nu\}. \tag{10}$$

With these essential elements of IGA spaces and basis functions, we can now introduce the IGA collocation method for the approximation of our acoustic wave problem in space, see Auricchio et al. [1] and [2], and Schillinger et al. [32]. Several choices of collocation points have been proposed in the literature, including Cauchy-Galerkin points in Gomez and De Lorenzis [18], Demko abscissae in Demko [11], Galerkin superconvergent points in Montardini et al. [26] and Greville abscissae in de Boor [10]. We will consider the set of Greville collocation points in our numerical experiments since it is one of the most used sets in the IGA collocation literature, and we refer to our previous work [37] for a numerical study of its stability and convergence properties for the approximation of acoustic wave problems. Given the knot vector $\{\xi_1 = 0, ..., \xi_{\nu+p+1} = 1\}$, the corresponding Greville collocation points are $\overline{\xi}_i \doteq (\xi_{i+1} + \xi_{i+2} + ... + \xi_{i+p})/p$ with $\overline{\xi}_1 = 0, \overline{\xi}_\nu = 1$, and the remaining points are in $(0, 1)$. The tensor product $\widehat{\tau}_{ij} = (\overline{\xi}_i, \overline{\xi}_j) \in \overline{(\widehat{\Omega})}$, $i, j = 1, ..., \nu$, provides the grid of collocation points $\tau_{ij} = \mathbf{F}(\widehat{\tau}_{ij}) \in \Omega$.

The theoretical analysis of spectral properties and convergence estimates for IGA collocation discretizations of elliptic problems in two and three dimensions is still an open issue. A large number of numerical tests are available in the literature regarding convergence properties with respect to the main discretization parameters, namely the degree p, the mesh size h and the regularity k (e.g., Auricchio et al. [1] and [2], Kruse et al. [25], Montardini et al. [26], Schillinger et al. [32] and our previous work [37]). In Section 5, we will present several numerical tests investigating the spectral properties of the matrices arising from IGA collocation methods for acoustic wave problems, including their eigenvalue distribution in the complex plane.

3.2 Space discretization of acoustic wave problems (1)-(4) by IGA collocation methods

For simplicity, we enumerate the grid points $\{\tau_{ij} \in \Omega,\ i, j = 1, ..., \nu\}$ using only one index. Thus, each collocation point τ_{ij} corresponds to one point P_k of the tensor product grid, with $k = 1, ..., \nu^2$. For clarity of exposition, we also introduce the following disjoint index sets: $\mathcal{I}_\Omega := \{k | P_k \in \Omega\}$ (internal points), $\mathcal{I}_D := \{k | P_k \in \Gamma_D\}$ (Dirichlet points), $\mathcal{I}_N := \{k | P_k \in \Gamma_N\}$ (Neumann points), $\mathcal{I}_{AB} := \{k | P_k \in \Gamma_{AB}\}$ (ABCs points), and define $\mathcal{I} := \mathcal{I}_\Omega \cup \mathcal{I}_D \cup \mathcal{I}_N \cup \mathcal{I}_{AB}$ as the set of ν^2 indexes of the whole mesh of collocation points. We can now write the IGA collocation semi-discrete continuous-in-time formulation of the acoustic problem (1)-(4) by collocating the continuous problem with initial and boundary conditions at the Greville collocation points:

$$\frac{\partial^2 u}{\partial t^2}(P_k, t) - c_0 \Delta u(P_k, t) = f(P_k, t), \qquad k \in \mathcal{I}_\Omega,\ t \in (0, T), \tag{11}$$

$$u(P_k, 0) = \mathcal{U}_0(P_k), \qquad \frac{\partial u}{\partial t}(P_k, 0) = \mathcal{W}_0(P_k), \qquad k \in \mathcal{I}, \tag{12}$$

$$u(P_k, t) = \Phi(P_k, t),\ k \in \mathcal{I}_D,\ t \in (0, T), \qquad \frac{\partial u}{\partial \mathbf{n}}(P_k, t) = \Psi(P_k, t),\ k \in \mathcal{I}_N,\ t \in (0, T) \tag{13}$$

$$\frac{1}{\sqrt{c_0}} \frac{\partial u}{\partial t}(P_k, t) + \frac{\partial u}{\partial \mathbf{n}}(P_k, t) = 0, \qquad k \in \mathcal{I}_{AB},\ t \in (0, T). \tag{14}$$

We observe that the semi-discrete collocation problem is equivalent to the problem of finding a vector $\mathbf{u}$ of elements $\{u_k,\ k \in \mathcal{I}\}$, which are in correspondence with elements $\{u_{ij},\ i, j = 1, ..., \nu\}$. From (9) and (10), the IGA numerical solution is then given by

$$u(\mathbf{x}, t) = \sum_{i,j=1}^{\nu} u_{ij} R_{ij}^p \circ \mathbf{F}^{-1}(\mathbf{x}, t). \tag{15}$$

In order to assemble the mass and stiffness IGA matrices, we introduce the IGA collocation matrices $[D_r]$, with $r = 0,\ 1,\ 2$, accounting for r-th derivative, respectively, at

the collocation points. Namely, we denote by D_0, D_1 and D_2 the collocation matrices associated to the identity, $\frac{\partial}{\partial \mathbf{n}}$ and Δ operators, respectively. See, e.g., Evans et al. [13]. We will refer to D_0 as the mass matrix and in Section 5, we will denote it by $\mathcal{M}$. Finally, the matrix form of the set of (11)-(14) can be rewritten as a system of second-order ordinary differential equations:

$$\frac{\partial^2}{\partial t^2}[D_0\mathbf{u}(t)]_k - c_0[D_2\mathbf{u}(t)]_k = [\mathbf{f}(t)]_k, \quad k \in \mathcal{I}_\Omega \tag{16}$$

$$[D_0\mathbf{u}(0)]_k = [\mathcal{U}_0]_k, \quad \frac{\partial}{\partial t}[D_0\mathbf{u}(0)]_k = [\mathcal{W}_0]_k, \quad k \in \mathcal{I}, \tag{17}$$

$$[D_0\mathbf{u}(t)]_k = [\mathbf{\Phi}(t)]_k, \quad k \in \mathcal{I}_D, \quad [D_1\mathbf{u}(t)]_k = [\mathbf{\Psi}(t)]_k, \quad k \in \mathcal{I}_N \tag{18}$$

$$\frac{1}{\sqrt{c_0}}\frac{\partial u}{\partial t}[D_0\mathbf{u}(t)]_k + [D_1\mathbf{u}(t)]_k = 0, \quad k \in \mathcal{I}_{AB} \tag{19}$$

where $[\mathbf{w}]_k$ is the k-th element of a general vector $\mathbf{w}$ and $[D_r]_k$ is the k-th row of the collocation matrix D_r, $r = 0, 1, 2$. Moreover, $\mathbf{u}(t) := \{u(P_k, t),\ k \in \mathcal{I}\}$, $\mathbf{f}(t) := \{f(P_k, t),\ k \in \mathcal{I}\}$, $\mathbf{\Phi}(t) := \{\Phi(P_k, t),\ k \in \mathcal{I}_D\}$, $\mathbf{\Psi}(t) := \{\Psi(P_k, t),\ k \in \mathcal{I}_N\}$, $\mathcal{U}_0 := \{\mathcal{U}_0(P_k),\ k \in \mathcal{I}\}$, $\mathcal{W}_0 := \{\mathcal{W}_0(P_k),\ k \in \mathcal{I}\}$, with all vectors equal to zero elsewhere.

3.3 Time discretization of acoustic wave problems (1)-(4) by Newmark advancing schemes

We discretize the time derivatives in (16), (17), and (19) by the finite difference scheme introduced by Newmark [28]. We first partition the interval $(0, T)$ into N subintervals $[t_n, t_{n+1}]$, with $t_0 = 0$, $t_N = T$, $t_{n+1} = t_n + \Delta t$, $n = 0, ..., N-1$ and $\Delta t = T/N$. Given real parameters $\beta \geq 0$ and $\gamma \geq 0$, the general form of Newmark method reads:

$$\mathbf{u}_{n+1} = \mathbf{u}_n + \Delta t\, \mathbf{v}_n + (1-2\beta)\Delta t^2 \mathbf{a}_n/2 + \beta \Delta t^2 \mathbf{a}_{n+1}, \quad \mathbf{v}_{n+1} = \mathbf{v}_n + (1-\gamma)\Delta t\, \mathbf{a}_n + \gamma \Delta t \mathbf{a}_{n+1}, \tag{20}$$

where $\mathbf{u}_n := \{u(P_k, t_n),\ k \in \mathcal{I}\}$, $\mathbf{v}_n := \{v(P_k, t_n),\ k \in \mathcal{I}\}$, $\mathbf{a}_n := \{a(P_k, t_n),\ k \in \mathcal{I}\}$ are the vectors of approximate displacement, velocity and acceleration, respectively, at time t_n. It can be shown (see, e.g., Wood [34] and [35]) that we can eliminate the velocity and acceleration vectors and express the Newmark method as a two-step scheme in the displacement term $\mathbf{u}_n$ only, whose entries give the corresponding IGA solution at time step t_n, according to (15). The initial vector $\mathbf{u}_1$ at the second time instant $t_1 = t_0 + \Delta t$, can be computed, for example, from the first one $\mathbf{u}_0$ associated with initial conditions (2) by means of a second-order explicit one-step method, (e.g., an explicit two-stage Runge–Kutta method), in order to preserve the global accuracy of the scheme. If we apply the Newmark scheme (20) to the numerical solution of the acoustic wave IGA collocation problem (16)-(19), we obtain the set of recurrence

relations for the displacement term $\mathbf{u}_n$ at the collocation points:

$$[D_0]_k \frac{\mathbf{u}_{n+1} - 2\mathbf{u}_n + \mathbf{u}_{n-1}}{\Delta t^2} - c_0 [D_2]_k \Big[\beta \mathbf{u}_{n+1} + \Big(\frac{1}{2} - 2\beta + \gamma\Big)\mathbf{u}_n + \Big(\frac{1}{2} + \beta - \gamma\Big)\mathbf{u}_{n-1}\Big] = \Big[\beta \mathbf{f}_{n+1} + \Big(\frac{1}{2} - 2\beta + \gamma\Big)\mathbf{f}_n + \Big(\frac{1}{2} + \beta - \gamma\Big)\mathbf{f}_{n-1}\Big]_k, \quad k \in \mathcal{I}_\Omega \tag{21}$$

$$[D_0]_k \mathbf{u}_{n+1} = [\mathbf{\Phi}(t_{n+1})]_k, \quad k \in \mathcal{I}_D, \quad [D_1]_k \mathbf{u}_{n+1} = [\mathbf{\Psi}(t_{n+1})]_k, \quad k \in \mathcal{I}_N \tag{22}$$

$$\frac{1}{\sqrt{c_0}} [D_0]_k \frac{\gamma \mathbf{u}_{n+1} + (1 - 2\gamma)\mathbf{u}_n + (\gamma - 1)\mathbf{u}_{n-1}}{\Delta t} + [D_1]_k \mathbf{u}_{n+1} = 0, \quad k \in \mathcal{I}_{AB}. \tag{23}$$

At corner points involving ABCs and/or Neumann boundary conditions, we enforce the average of normal derivatives, whereas Dirichlet conditions override Neumann or ABC ones. With suitable generalizations of coefficients multiplying the matrices D_0 and D_1 in (23), we note that the approximation of ABCs is mathematically equivalent to that of the most common Robin boundary conditions, involving a linear combination of the values of a function and of its normal derivative at the collocation points on the boundary.

The scheme (21) is customarily considered explicit when $\beta = 0$, even if the matrix D_0 is not diagonal. More generally, regardless of the parameter β, we observe that each step of (21)-(23) involves the resolution of a linear system $\mathcal{K}\mathbf{u}_{n+1} = \mathbf{\Upsilon}(t_{n+1}, t_n, t_{n-1})$, where the IGA collocation iteration matrix

$$\mathcal{K} = [D_0]_{k \in \mathcal{I}_D} + [D_1]_{k \in \mathcal{I}_N \cup \mathcal{I}_{AB}} + \frac{\gamma}{\Delta t \sqrt{c_0}} [D_0]_{k \in \mathcal{I}_{AB}} - c_0 \beta [D_2]_{k \in \mathcal{I}_\Omega} + \frac{1}{\Delta t^2} [D_0]_{k \in \mathcal{I}_\Omega}, \tag{24}$$

is non-symmetric and becomes denser for increasing p and k, both for explicit ($\beta = 0$) and implicit ($\beta \neq 0$) methods, independently of the boundary conditions considered. We note that in the explicit case ($\beta = 0$), the iteration matrix $\mathcal{K}$ is essentially equal to the mass matrix modified by the boundary conditions. Finally, the right term $\mathbf{\Upsilon}(t_{n+1}, t_n, t_{n-1})$ accounts for the values of data functions $\mathcal{U}_0$, $\mathcal{W}_0$, f, Φ and Ψ at times t_{n+1}, t_n, t_{n-1}.

4 Condition number estimates

We recall the condition number estimates that have been proven in Gahalaut and Tomar [14] in the two-dimensional case for the Galerkin isogeometric mass ($\mathcal{M}$) and stiffness ($\mathcal{A}$) matrices, regardless of the k-regularity of the spline basis functions:

$$cond(\mathcal{M}) \leq c p^2 16^p, \quad \text{with } c \text{ independent of } h \text{ and } p, \tag{25}$$

$$cond(\mathcal{A}) \leq c(h) p^8 16^p. \tag{26}$$

In addition, some bounds on the smallest and largest eigenvalues are proven in Gahalaut and Tomar [14] in the one-dimensional case, and in Garoni et al. [15] also for the case of dimension $d > 1$. A systematic numerical study has been accomplished in

Gervasio et al. [16] in order to investigate experimentally the conditioning of Galerkin isogeometric mass and stiffness matrices in d dimensions, resulting in the following more detailed and sharper estimates:

$$\text{for } k = 0 \text{ regularity:} \quad cond(\mathcal{M}) \approx p^{-d/2} 4^{pd}, \tag{27}$$

$$\text{for } k = p-1 \text{ regularity:} \quad cond(\mathcal{M}) \approx \begin{cases} e^{pd} & \text{if } h \leq 1/p \\ (e/4)^{d/h} (hp)^{-d/2} 4^{pd} & \text{otherwise,} \end{cases} \tag{28}$$

$$\text{for } k = 0 \text{ regularity:} \quad cond(\mathcal{A}) \approx \begin{cases} h^{-2} p^2 & \text{if } h \leq (p^{2+d/2} d^{-dp})^{1/2} \\ p^{-d/2} 4^{pd} & \text{otherwise,} \end{cases} \tag{29}$$

$$\text{for } k = p-1 \text{ regularity:} \quad cond(\mathcal{A}) \approx \begin{cases} h^{-2} p & \text{if } h \leq e^{-dp/2} \\ p e^{pd} & \text{if } e^{-dp/2} \leq h \leq 1/p \\ (e/4)^{d/h} p^{-d/2} h^{-d/2-1} 4^{pd} & \text{otherwise.} \end{cases} \tag{30}$$

The numerical results reported in the next section show that estimates (27)–(30) hold also for the condition number of the collocation isogeometric mass and iteration matrices considered in this work, and, what's more, in some cases the collocation matrices satisfy improved bounds. In particular, the term 4^{pd} appearing in these estimates seems to reduce in the two-dimensional case ($d = 2$) to at least $4^{\frac{3}{2}p}$, and in some cases for sufficiently small h to 4^p or even $4^{\frac{1}{2}p}$.

5 Numerical results

In this section, we present a numerical study of the behavior of the eigenvalues and condition numbers of the mass matrix $\mathcal{M}$ and iteration matrix $\mathcal{K}$ for the acoustic wave problem in the reference square domain $\Omega = [0, 1] \times [0, 1]$ with different types of boundary conditions. We vary the degree p, regularity k, and mesh size h for the IGA collocation method introduced in Section 3.2, and the discretization parameters Δt and β of the Newmark time-advancing scheme introduced in Section 3.3. We denote by d.o.f. the number of degrees of freedom of the discrete problem and by nz the number of nonzero entries in the mass and iteration matrices. All tests have been carried out in 2D with MATLAB R2020b and using the GeoPDEs 3.0 library written by De Falco et al. [9] and Vázquez [33]. In particular, the construction of the collocation matrices introduced in Section 3.2 is based on the structure `sp_eval`, whereas the condition numbers are computed using the MATLAB `condest` function (denoted by continuous lines and $\circ$ symbols in the plot) or computed as the ratio $|\lambda_{max}|/|\lambda_{min}|$ (denoted by dashed lines and $\star$ symbols in the plots), where the MATLAB `condest` function approximates the 1-norm condition number of a square matrix. In all our tests, the last ratio is always bounded from above by `condest`, and since both condition number estimates show the same qualitative behavior in h, p, k, we report both estimates only in the plots in h (top rows) in Figs. 1, 6, 9, and 10, while we report only `condest` in the other plots in p and k.

Eigenvalues and condition number of the mass matrix In Fig. 1, we report the condition numbers $\mathsf{cond}(\mathcal{M})$ of the mass matrix versus: the mesh size h (top), with five different values of degree p and minimal regularity $k = 1$ (left), or maximal regularity $k = p - 1$ (right); the degree p (center), with five different values of mesh size h and minimal regularity $k = 1$ (left), or maximal regularity $k = p - 1$ (right); the regularity k (bottom), with three different values of mesh size h, fixed $p = 12$. In the h-refinement test (top), the condition numbers $\mathsf{cond}(\mathcal{M})$ are independent of h, whereas

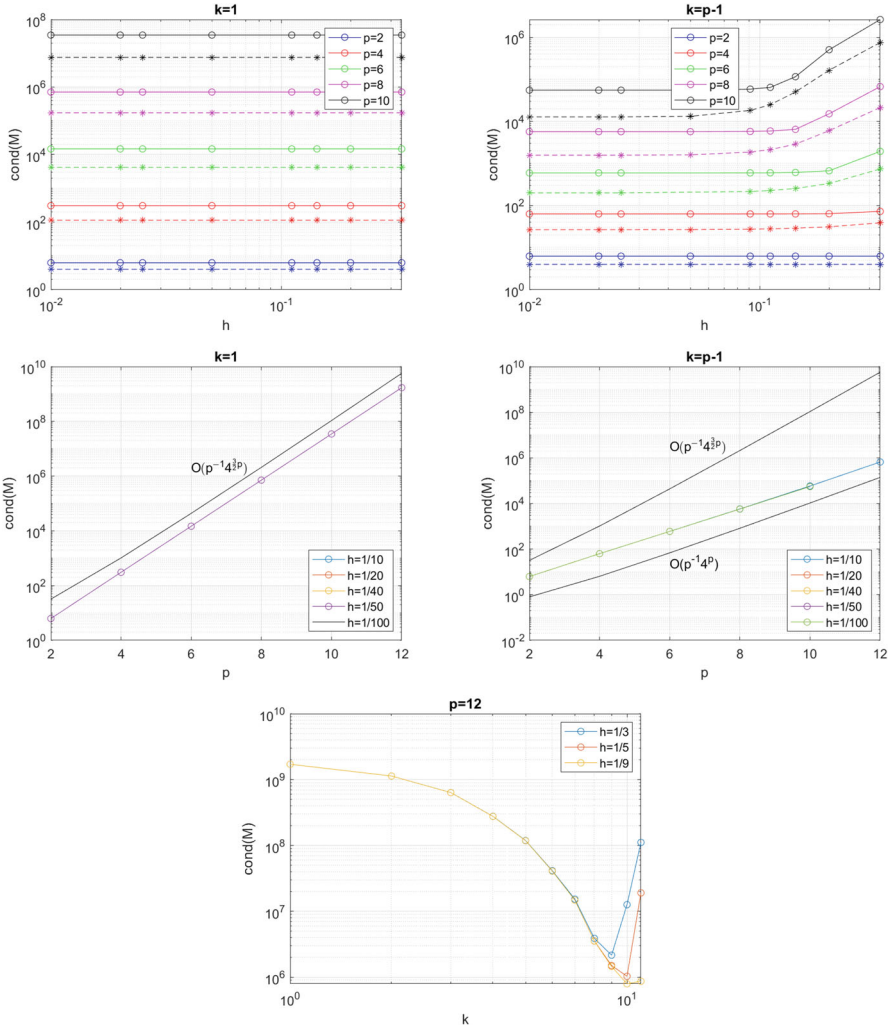

Fig. 1 Condition number $\mathsf{cond}(\mathcal{M})$ of the mass matrix versus: h (top), for $p = 2,\ 4,\ 6,\ 8,\ 10$, $k = 1$ (left), or $k = p - 1$ (right); p (center), for $h = 1/10,\ 1/20,\ 1/40,\ 1/50,\ 1/100$, $k = 1$ (left), or $k = p - 1$ (right); k (bottom), for $h = 1/3,\ 1/5,\ 1/9$, fixed $p = 12$. Continuous lines with $\circ$ symbols denote condition numbers computed with Matlab `condest` function, dashed lines with $\star$ symbols denote condition numbers computed as the ratio $|\lambda_{max}|/|\lambda_{min}|$

they grow slower than the estimates (27)-(28) for p- refinement. In the p-refinement test (center), and independently of the selected h, the condition numbers $\mathsf{cond}(\mathcal{M})$ for minimal regularity $k = 1$ (center left) appear to grow like $O(p^{-1}4^{3p/2})$, slightly better than the $O(p^{-1}4^{2p})$ predicted by (27). In the case of maximal regularity $k = p - 1$ (center right), the growth of $\mathsf{cond}(\mathcal{M})$ is between $O(p^{-1}4^{p})$ and $O(p^{-1}4^{3p/2})$, again slightly better than the growth predicted by (28).

For increasing k (bottom), fixed p and h, $\mathsf{cond}(\mathcal{M})$ seem to decrease exponentially except when the regularity k approaches the maximum value $p - 1$ and $\mathsf{cond}(\mathcal{M})$ increase sharply toward the midpoint of $\mathsf{cond}(\mathcal{M})$ range.

Figure 2 reports the mass matrix $\mathcal{M}$ eigenvalue distribution in the complex plane for three different values of degree $p = 4$ (left), $p = 8$ (center), $p = 12$ (right), for fixed $h = 1/10$, minimal regularity $k = 1$ (top), or $h = 1/100$, maximal regularity $k = p-1$ (bottom), whereas in Fig. 3, we report the eigenvalue distribution for three different values of mesh size $h = 1/25$ (left), $h = 1/40$ (center), $h = 1/50$ (right), minimal regularity $k = 1$ (top), or $h = 1/40$ (left), $h = 1/50$ (center), $h = 1/100$ (right), maximal regularity $k = p - 1$ (bottom), for fixed $p = 4$. In all cases, the eigenvalues are essentially real, since their imaginary parts are of the order of machine precision, and their real parts are in the interval $[0,\ 1]$.

Figure 4 shows the sparsity pattern of the mass matrix $\mathcal{M}$ for three different values of degree $p = 4$ (left), $p = 8$ (center), $p = 12$ (right), minimal regularity $k = 1$ (top), or maximal regularity $k = p - 1$ (bottom), for fixed $h = 1/5$, whereas in Fig. 5, we report the sparsity pattern for three different values of mesh size $h = 1/3$ (left), $h = 1/7$ (center), $h = 1/11$ (right), minimal regularity $k = 1$ (top), or maximal regularity $k = p - 1$ (bottom), for fixed $p = 8$. The number of d.o.f. and nonzero elements nz decrease considerably when the regularity is increased from minimal to maximal, and the difference grows when p or $1/h$ is increased.

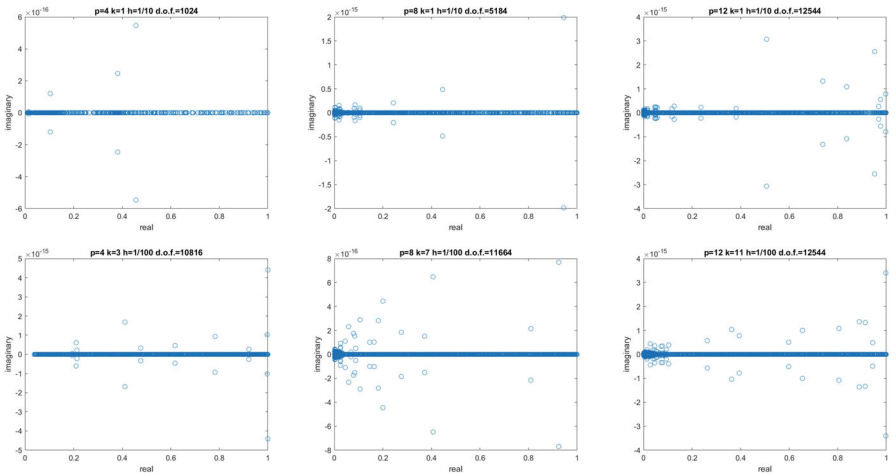

Fig. 2 Mass matrix eigenvalue distribution in the complex plane, for $p = 4$ (left), $p = 8$ (center), $p = 12$ (right), with $h = 1/10$ and $k = 1$, (top), or with $h = 1/100$ and $k = p - 1$ (bottom)

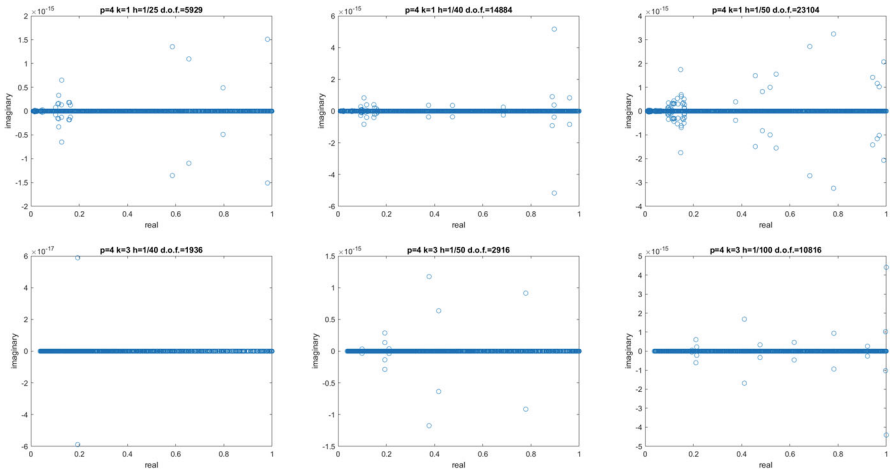

Fig. 3 Mass matrix eigenvalue distribution in the complex plane, fixed $p = 4$, for $h = 1/25$ (left), $1/h = 40$ (center), $1/h = 50$ (right), with $k = 1$ (top), or $h = 1/40$ (left), $1/h = 50$ (center), $1/h = 100$ (right), with $k = p - 1$ (bottom)

Eigenvalues and condition number of the iteration matrix with Dirichlet and Neumann boundary conditions

In Fig. 6, we report the condition numbers $\mathsf{cond}(\mathcal{K})$ of the iteration matrix for the acoustic wave problem with Dirichlet boundary conditions, for $\Delta t = 0.1$, $\beta = 0$ (explicit Newmark scheme, left), or $\beta = 0.5$ (implicit Newmark scheme, right), versus, from the top to the bottom: (1) the mesh size h, with five different values of degree p and minimal regularity $k = 1$, (2) the mesh size h, with five different values of

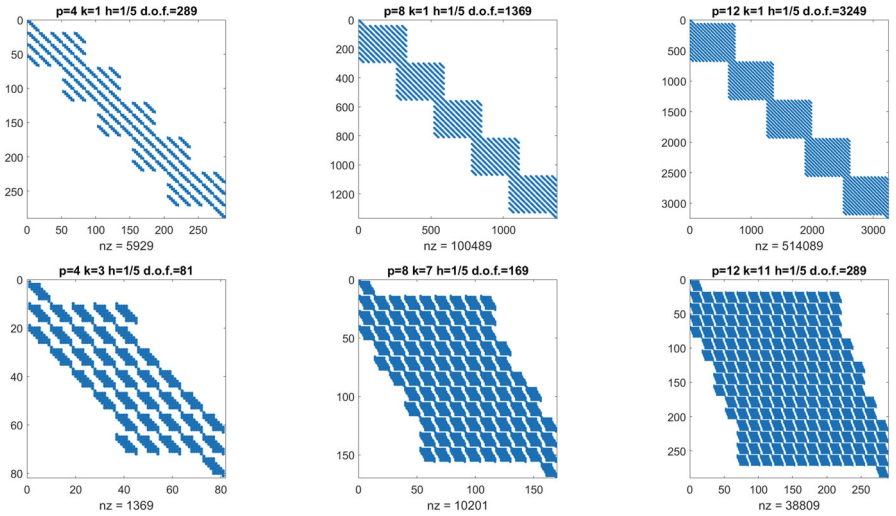

Fig. 4 Mass matrix sparsity pattern, for $p = 4$ (left), $p = 8$ (center), $p = 12$ (right), with $k = 1$ (top), or $k = p - 1$ (bottom), fixed $h = 1/5$

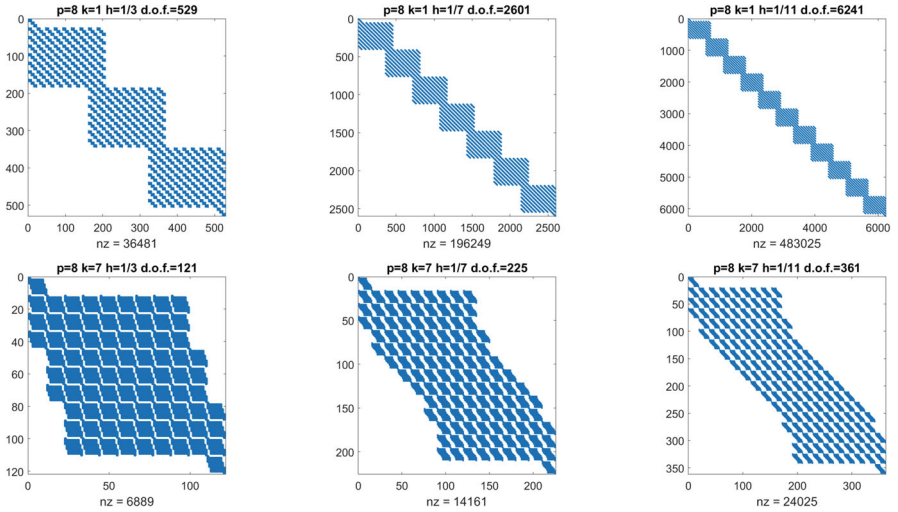

Fig. 5 Mass matrix sparsity pattern, for $h = 1/3$ (left), $1/h = 7$ (center), $1/h = 11$ (right), with $k = 1$ (top), or $k = p - 1$ (bottom), fixed $p = 8$

degree p and maximal regularity $k = p - 1$, (3) the degree p, with four different values of mesh size h and minimal regularity $k = 1$, (4) the degree p, with four different values of mesh size h and maximal regularity $k = p - 1$. We have also run the same tests as in Fig. 6 but with a smaller time step $\Delta t = 0.01$ (not shown for brevity). The numerical results show that if p is fixed, the condition numbers $\mathsf{cond}(\mathcal{K})$ are almost always independent of h for the explicit scheme (left), while they seem to grow as h^{-2}, for the implicit scheme (right), in agreement with estimates (29)-(30). For the p- refinement with fixed h, it seems that the numerical results are better than these estimates. Indeed, the condition number $\mathsf{cond}(\mathcal{K})$ growth ranges between $p^{-1}4^p$ and $p^{-1}4^{\frac{3}{2}p}$ in the case of minimal regularity $k = 1$, whereas for maximal regularity $k = p-1$ the growth ranges between $p^{-1}4^{\frac{1}{2}p}$ and $p^{-1}4^p$. We have also run analogous tests for the acoustic wave problem with Neumann boundary conditions (not shown for brevity), obtaining analogous results in h and p, for both $\Delta t = 0.1$ and $\Delta t = 0.01$.

Figure 7 reports the iteration matrix $\mathcal{K}$ eigenvalue distribution in the complex plane for the acoustic wave problem with Dirichlet boundary conditions, $\Delta t = 0.01$, $\gamma = 0.5$, $\beta = 0.5$ (implicit Newmark scheme), for three different values of degree $p = 4$ (left), $p = 8$ (center), $p = 12$ (right), for fixed $h = 1/10$ and minimal regularity $k = 1$ (top), or fixed $h = 1/100$ and maximal regularity $k = p - 1$ (bottom), whereas in Fig. 8, we report the eigenvalue distribution for three different values of mesh size $h = 1/25$ (left), $h = 1/40$ (center), $h = 1/50$ (right), minimal regularity $k = 1$ (top), or $h = 1/40$ (left), $h = 1/50$ (center), $h = 1/100$ (right), maximal regularity $k = p-1$ (bottom), for fixed $p = 4$ in both cases. The eigenvalues real parts belong to an interval $[0, r]$ where r increases with $1/h$, fixed p, and with p, fixed $1/h$, for both minimal regularity $k = 1$ and maximal regularity $k = p - 1$. We note the presence of a few complex outliers.

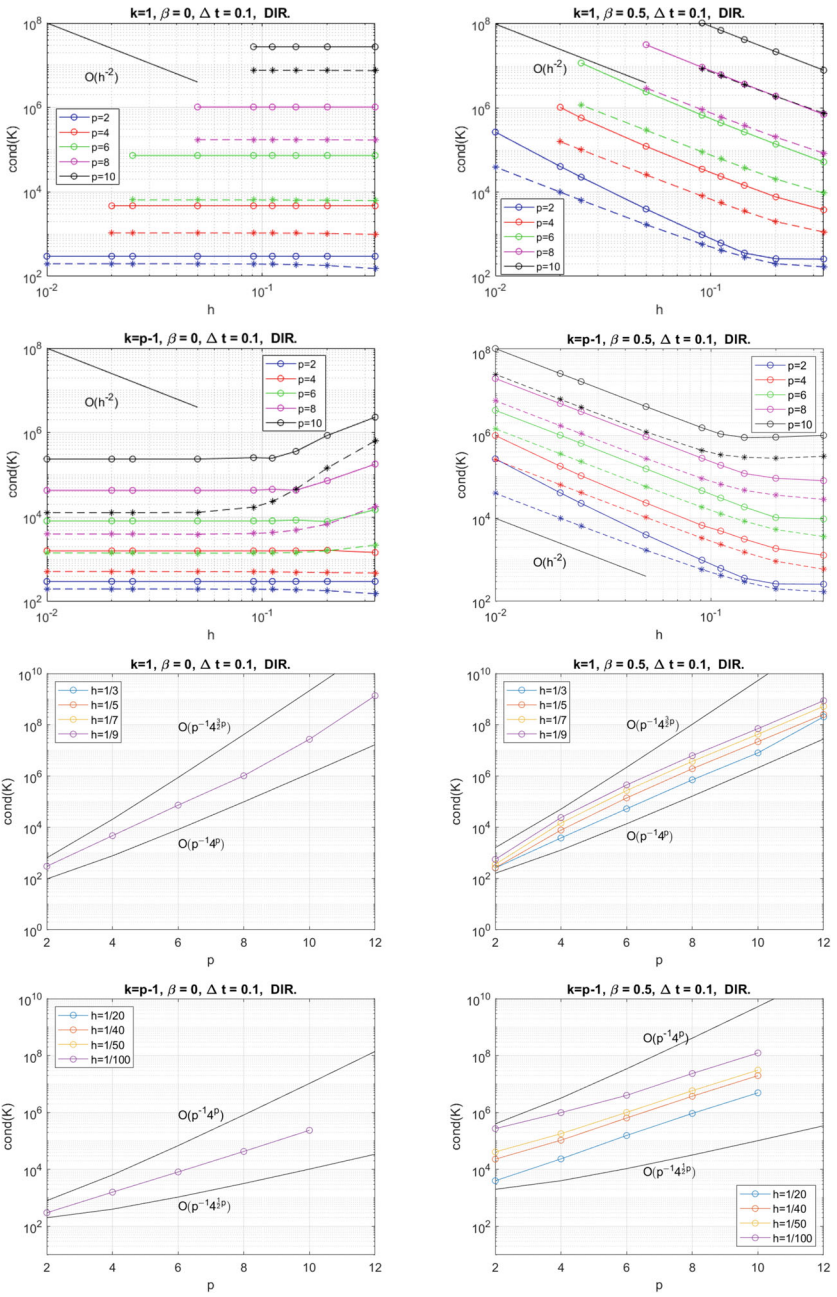

Fig. 6 Condition number cond($\mathcal{K}$) of the iteration matrix for the acoustic wave problem with Dirichlet boundary conditions, $\Delta t = 0.1$, $\gamma = 0.5$, $\beta = 0$ (explicit Newmark, left), $\beta = 0.5$ (implicit Newmark, right). From the top to the bottom, vs.: (1) h, for $p = 2, 4, 6, 8, 10$, $k = 1$; (2) h, for $p = 2, 4, 6, 8, 10$, $k = p - 1$; (3) p, for $h = 1/3, 1/5, 1/7, 1/9$, $k = 1$; (4) p, for $h = 1/20, 1/40, 1/50, 1/100$, $k = p - 1$. Continuous lines with $\circ$ symbols denote condition numbers computed with Matlab `condest` function, dashed lines with $\star$ symbols denote condition numbers computed as the ratio $|\lambda_{max}|/|\lambda_{min}|$

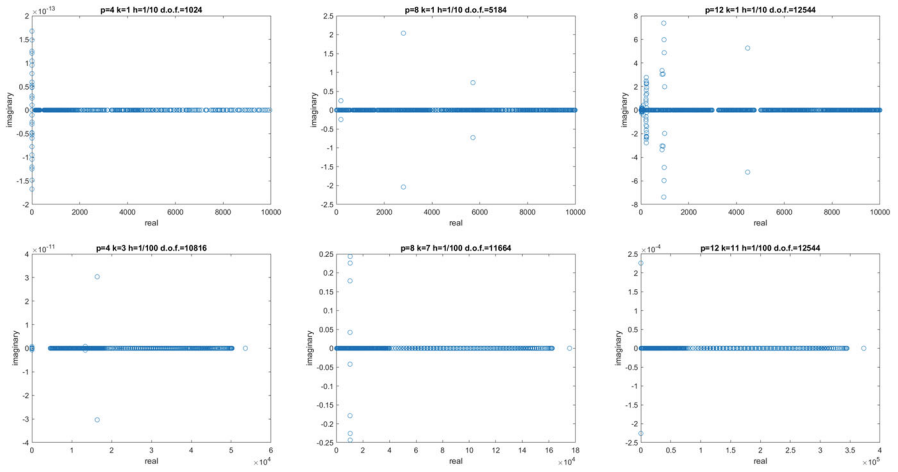

Fig. 7 Iteration matrix eigenvalue distribution in the complex plane for the acoustic wave problem with Dirichlet boundary conditions: for $p = 4$ (left), $p = 8$ (center), $p = 12$ (right), with $h = 1/10$ and $k = 1$ (top), or with $h = 1/100$ and $k = p - 1$ (bottom); fixed $\Delta t = 0.01$, $\gamma = 0.5$, $\beta = 0.5$ (implicit)

The sparsity pattern of the iteration matrix $\mathcal{K}$ are analogous to those for the mass matrices in Figs. 4 and 5, with block-diagonal matrices for minimal regularity and almost dense matrices in the case of maximal regularity. Again, both d.o.f. and nz decrease for increasing regularity.

Eigenvalues and condition number of the iteration matrix with absorbing boundary conditions In Figs. 9 ($\Delta t = 0.1$) and 10 ($\Delta t = 0.01$), we report the

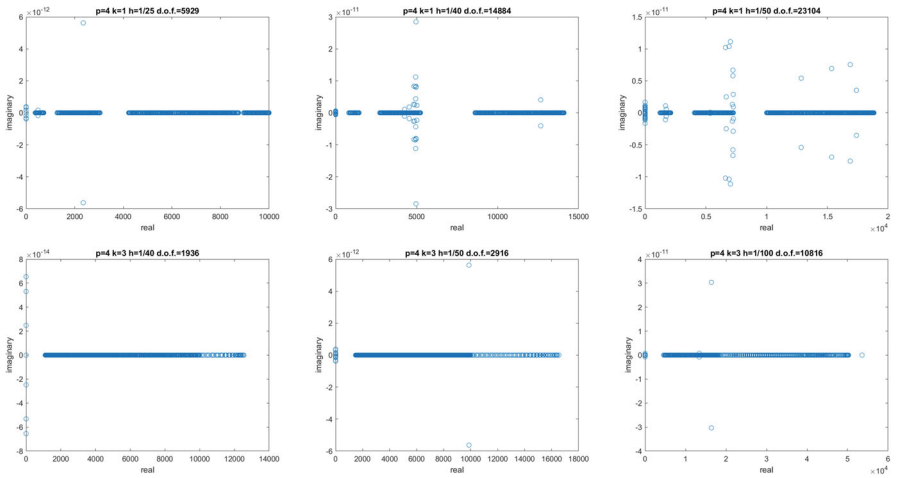

Fig. 8 Iteration matrix eigenvalue distribution in the complex plane for the acoustic wave problem with Dirichlet boundary conditions: for $h = 1/25$ (left), $1/h = 40$ (center), $1/h = 50$ (right), with $k = 1$ (top), or $h = 1/40$ (left), $1/h = 50$ (center), $1/h = 100$ (right), with $k = p-1$ (bottom); fixed $p = 4$, $\Delta t = 0.01$, $\gamma = 0.5$, $\beta = 0.5$ (implicit)

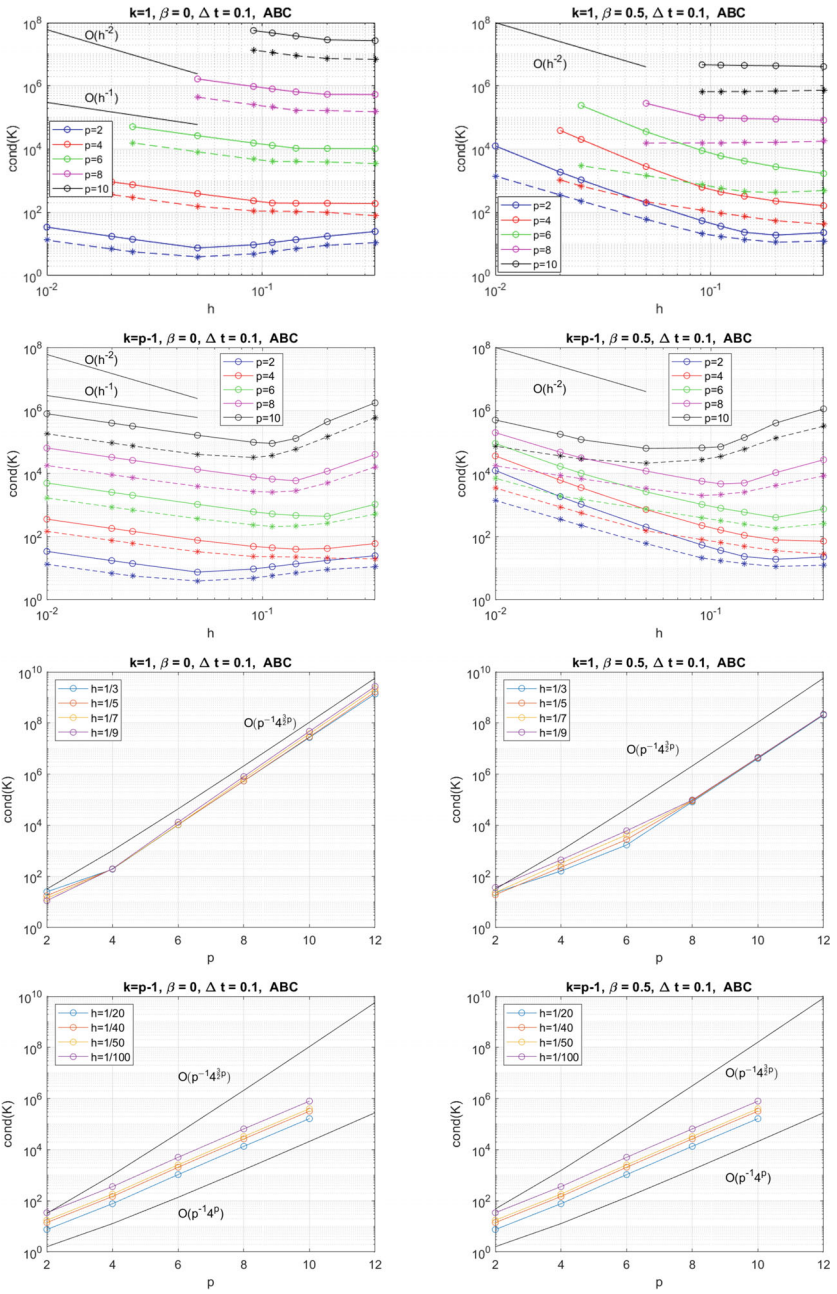

Fig. 9 Condition number cond($\mathcal{K}$) of the iteration matrix for the acoustic wave problem with absorbing boundary conditions (4), $\Delta t = 0.1$, $\gamma = 0.5$, $\beta = 0$ (explicit Newmark, left), $\beta = 0.5$ (implicit Newmark, right). From the top to the bottom, vs.: (1) h, for $p = 2, 4, 6, 8, 10$, $k = 1$; (2) h, for $p = 2, 4, 6, 8, 10$, $k = p - 1$; (3) p, for $h = 1/3, 1/5, 1/7, 1/9$, $k = 1$; (4) p, for $h = 1/20, 1/40, 1/50, 1/100$, $k = p - 1$. Continuous lines with $\circ$ symbols denote condition numbers computed with Matlab `condest` function, dashed lines with $\star$ symbols denote condition numbers computed as the ratio $|\lambda_{max}|/|\lambda_{min}|$

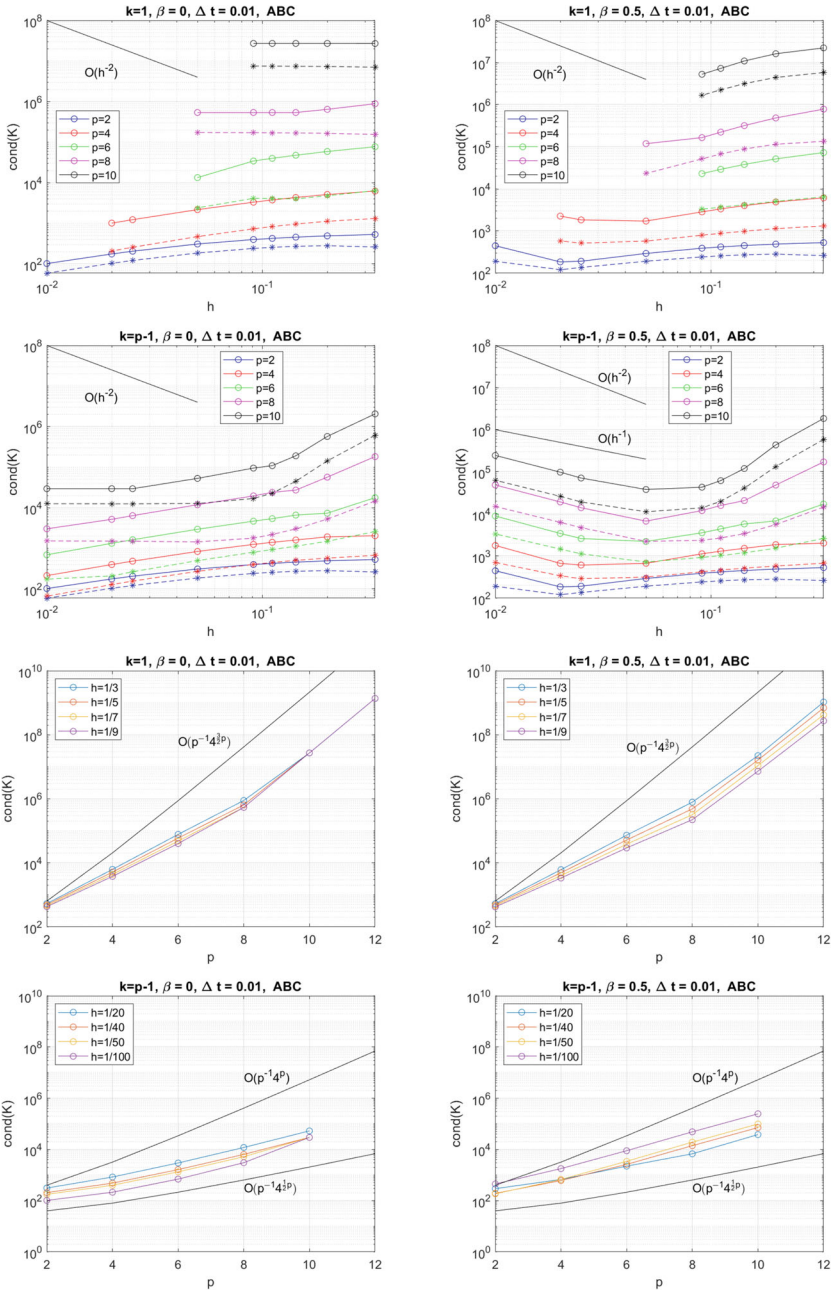

Fig. 10 Condition number cond($\mathcal{K}$) of the iteration matrix for the acoustic wave problem with absorbing boundary conditions (4), $\Delta t = 0.01, \gamma = 0.5, \beta = 0$ (explicit Newmark, left), $\beta = 0.5$ (implicit Newmark, right). From the top to the bottom, vs.: (1) h, for $p = 2, 4, 6, 8, 10$, $k = 1$; (2) h, for $p = 2, 4, 6, 8, 10$, $k = p - 1$; (3) p, for $h = 1/3, 1/5, 1/7, 1/9$, $k = 1$; (4) p, for $h = 1/20, 1/40, 1/50, 1/100$, $k = p - 1$. Continuous lines with $\circ$ symbols denote condition numbers computed with Matlab `condest` function, dashed lines with $\star$ symbols denote condition numbers computed as the ratio $|\lambda_{max}|/|\lambda_{min}|$

condition numbers $\mathsf{cond}(\mathcal{K})$ of the iteration matrix for the acoustic wave problem with absorbing boundary conditions (4), using the same setting of Fig. 6.

The numerical results in Fig. 9 ($\Delta t = 0.1$) for h-refinement with p fixed, show that the condition numbers $\mathsf{cond}(\mathcal{K})$ for the implicit scheme (right) are constant or decreasing for larger h, but when h decreases $\mathsf{cond}(\mathcal{K})$ seem to grow as h^{-2}, in agreement with estimates (29)-(30). The results for the explicit scheme (left) are analogous but the growth of $\mathsf{cond}(\mathcal{K})$ for decreasing h seems to be $O(h^{-1})$ instead of $O(h^{-2})$, as it can be expected from the presence of first-order term D_1 in (24). The situation is less clear for the analogous h-refinement tests with smaller time step $\Delta t = 0.01$ in Fig. 10. Here the condition numbers $\mathsf{cond}(\mathcal{K})$ for the explicit scheme (left) are constant or decreasing for all values of h considered, while for the implicit scheme (right) $\mathsf{cond}(\mathcal{K})$ start increasing as $O(h^{-1})$ only for small values of h. The results in Fig. 9 for p- refinement with fixed h and $\Delta t = 0.1$ show that the condition numbers $\mathsf{cond}(\mathcal{K})$ are better than the estimates (29)-(30) since the $\mathsf{cond}(\mathcal{K})$ growth ranges between $p^{-1}4^p$ and $p^{-1}4^{\frac{3}{2}p}$, while the results in Fig. 10 improve for $\Delta t = 0.01$, as the growth ranges between $p^{-1}4^{\frac{1}{2}p}$ and $p^{-1}4^p$.

In Fig. 11, we report the condition numbers $\mathsf{cond}(\mathcal{K})$ of the iteration matrix as a function of the regularity k. We consider different types of boundary conditions: absorbing (top), Dirichlet (center), Neumann (bottom), and choose $\beta = 0$ (explicit Newmark), $\gamma = 0.5$, degree $p = 12$, $\Delta t = 0.1$ (left), or $\Delta t = 0.01$ (right), and three different values of mesh size h. The results are analogous to those for the mass matrices in Fig. 1 for each type of boundary condition: when k increases, $\mathsf{cond}(\mathcal{K})$ start to decrease exponentially, but when the regularity k approaches the maximum value $p - 1$ $\mathsf{cond}(\mathcal{K})$ increase sharply toward the midpoint of $\mathsf{cond}(\mathcal{K})$ range.

In Figs. 12 and 13, we report the iteration matrix $\mathcal{K}$ eigenvalue distribution in complex plane for the acoustic wave problem with absorbing boundary conditions, and explicit Newmark scheme ($\beta = 0$), for $\Delta t = 0.01$ and $\gamma = 0.5$, using the same setting of Figs. 7 and 8, respectively. We see that the eigenvalues real parts belong to an interval $[0, r]$ with r independent of all parameters h, p, and k. The complex eigenvalues have imaginary parts that belong to an interval $[-s, s]$ where s increases with $1/h$, fixed p, and with p, fixed $1/h$. We note the presence of a few complex outliers close to the imaginary axis.

In Figs. 14 and 15, we report the same data as in Figs. 12, 13, respectively, but for the implicit Newmark scheme ($\beta = 0.5$), all other values of parameters being unchanged. We observe definitely fewer complex eigenvalues, but some complex outliers are still present. The eigenvalue distributions remain confined in a complex box $[0, r] \times [-s, s]$, with r increasing with $1/h$ and p, for both minimal regularity $k = 1$ and maximal regularity $k = p - 1$.

6 Conclusions

In this paper, we have investigated the spectral properties of the mass and iteration matrices related to the approximation of the acoustic wave equation with Dirichlet, Neumann and absorbing boundary conditions in the reference square domain by IGA

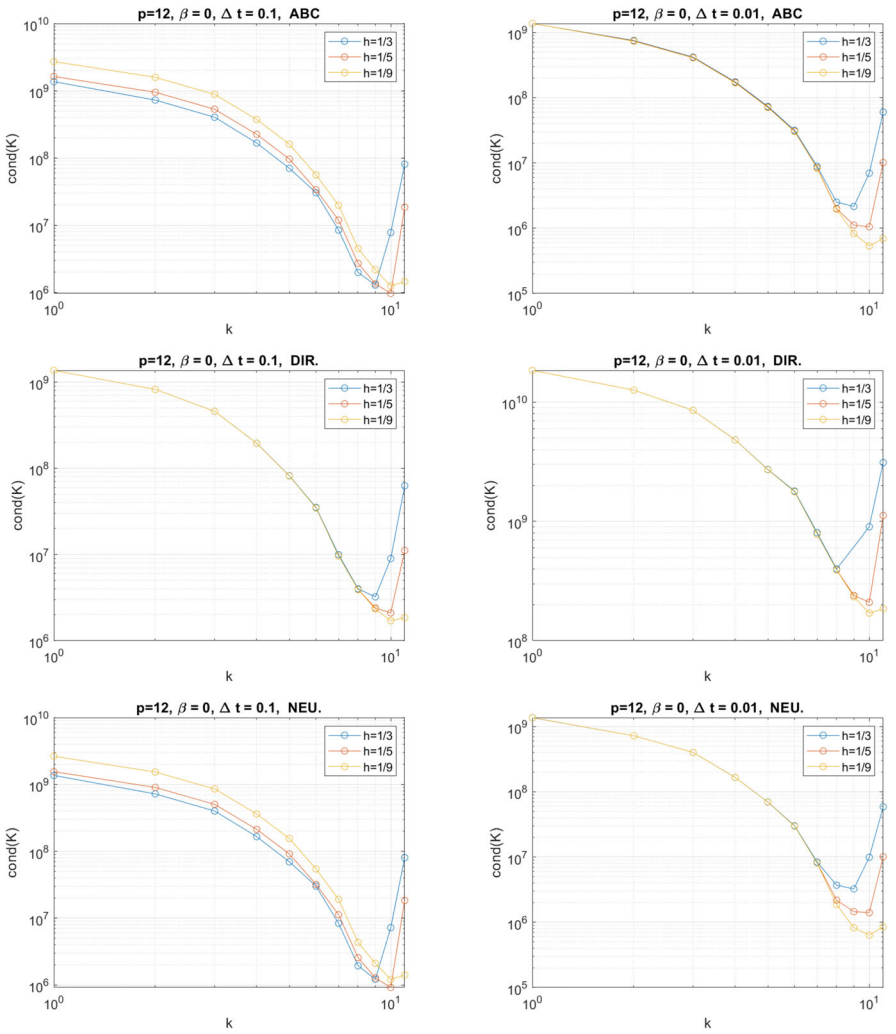

Fig. 11 Condition numbers $\mathsf{cond}(\mathcal{K})$ of the iteration matrix for the acoustic wave problem with different types of boundary conditions: absorbing (top), Dirichlet (center), Neumann (bottom), as a function of k, $\beta = 0$ (explicit Newmark), $\gamma = 0.5$, degree $p = 12$, $\Delta t = 0.1$ (left) and $\Delta t = 0.01$ (right), $h = 1/3,\ 1/5,\ 1/9$

collocation methods in space and Newmark advancing schemes in time, both explicit and implicit. Since no theoretical results are yet available in the literature for the spectral properties of IGA collocation matrices, we have conducted a systematic numerical study of the eigenvalue distribution, condition numbers, and sparsity of the mass and iteration matrices varying the parameters p, h, k, for the space discretization and Δt, β for the time discretization.

This analysis is of interest not only in order to estimate the maximum allowable time step Δt for explicit Newmark schemes, but also for the possible investigation of efficient preconditioned iterative solutions of the linear systems arising at each step

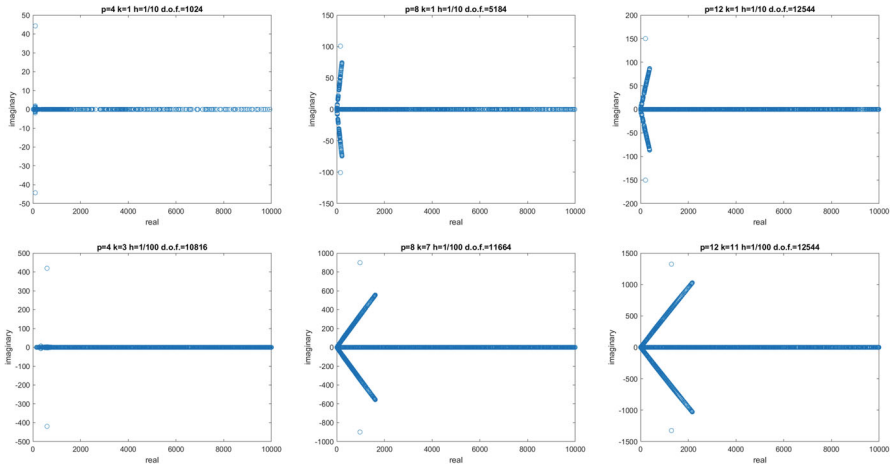

Fig. 12 Iteration matrix eigenvalue distribution in the complex plane for the acoustic wave problem with absorbing boundary conditions and explicit Newmark scheme ($\beta = 0$): for $p = 4$ (left), $p = 8$ (center), $p = 12$ (right), with $h = 1/10$ and $k = 1$ (top), or with $h = 1/100$ and $k = p - 1$ (bottom); fixed $\Delta t = 0.01$, $\gamma = 0.5$

of the time-advancing schemes, since the corresponding matrices are non-symmetric and become denser for increasing p and k, for both explicit and implicit methods.

Despite the lack of proven collocation bounds and estimates, we have compared the results of our tests with the theory and numerical results available for matrices resulting from the IGA Galerkin approximation of the Laplacian with Dirichlet boundary conditions. Our results show that analogous estimates for the condition numbers of

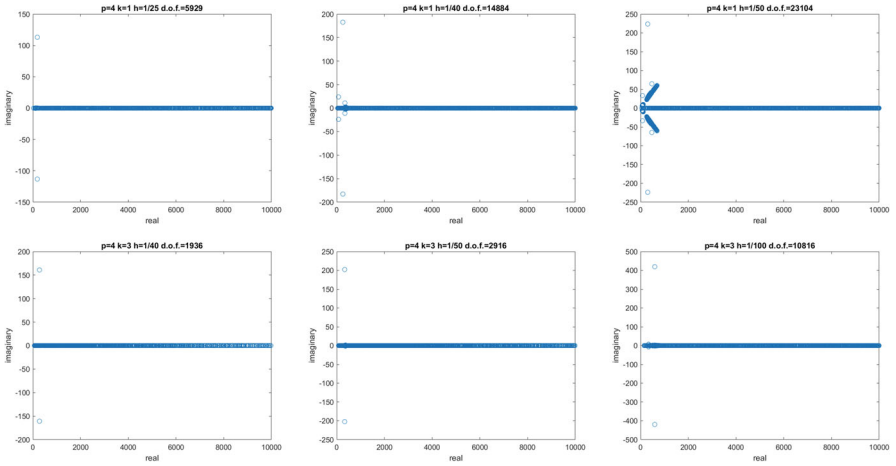

Fig. 13 Iteration matrix eigenvalue distribution in the complex plane for the acoustic wave problem with absorbing boundary conditions and explicit Newmark scheme ($\beta = 0$): for $h = 1/25$ (left), $1/h = 40$ (center), $1/h = 50$ (right), with $k = 1$ (top), or $h = 1/40$ (left), $1/h = 50$ (center), $1/h = 100$ (right), with $k = p - 1$ (bottom); fixed $p = 4$, $\Delta t = 0.01$, $\gamma = 0.5$

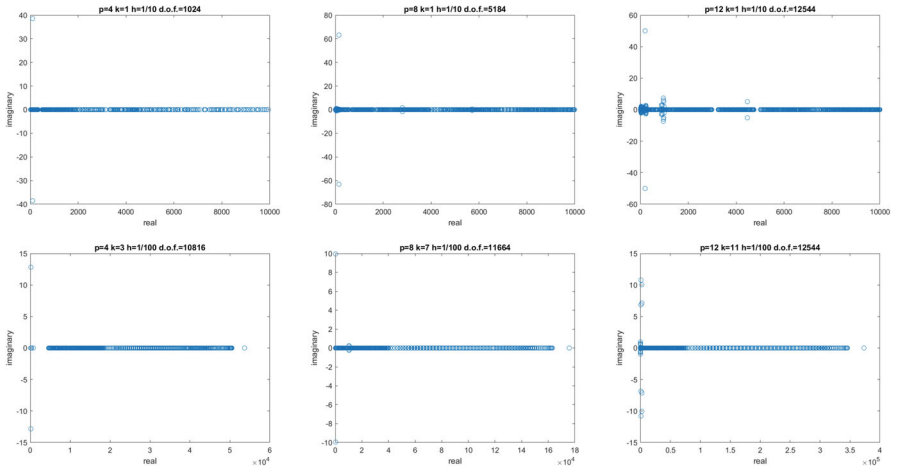

Fig. 14 Iteration matrix eigenvalue distribution in the complex plane for the acoustic wave problem with absorbing boundary conditions and implicit Newmark scheme ($\beta = 0.5$): for $p = 4$ (left), $p = 8$ (center), $p = 12$ (right), with $h = 1/10$ and $k = 1$ (top), or with $h = 1/100$ and $k = p - 1$ (bottom); fixed $\Delta t = 0.01$, $\gamma = 0.5$

mass and iteration matrices hold also for IGA collocation discretizations of acoustic wave problems, and in some cases, the collocation bounds are better than the Galerkin ones, in particular for increasing p and maximal regularity $k = p - 1$.

Limitations and future work This study was confined to acoustic wave problems in the reference square, but we do not expect different trends and technical complexity in extending the tests to three-dimensional domains, by using the tensor product structure of IGA collocation.

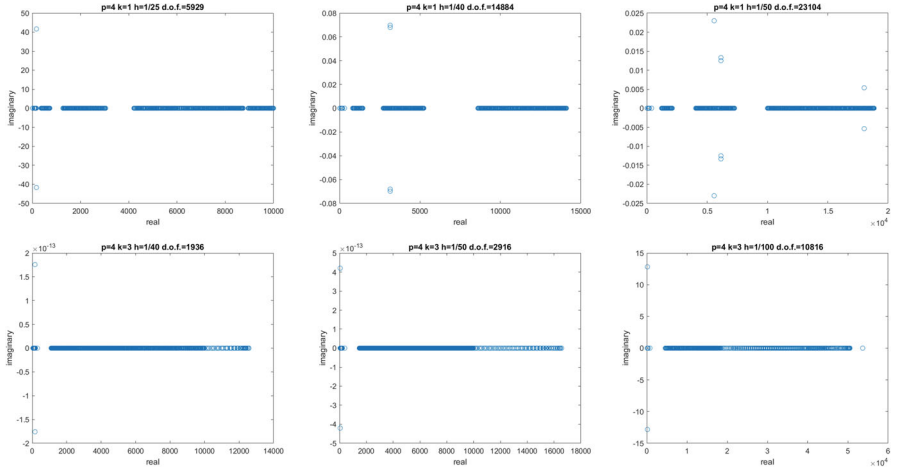

Fig. 15 Iteration matrix eigenvalue distribution in the complex plane for the acoustic wave problem with absorbing boundary conditions and implicit Newmark scheme ($\beta = 0.5$): for $h = 1/25$ (left), $1/h = 40$ (center), $1/h = 50$ (right), with $k = 1$ (top), or $h = 1/40$ (left), $1/h = 50$ (center), $1/h = 100$ (right), with $k = p - 1$ (bottom); fixed $p = 4$, $\Delta t = 0.01$, $\gamma = 0.5$

Future work will consider the issue of preconditioning the linear systems arising at each time step, as well as the extension of this work to elastic wave problems.

Funding Open access funding provided by Università degli Studi di Milano within the CRUI-CARE Agreement. This work was partially supported by the European Research Council through the FP7 Ideas Consolidator Grant *HIGEOM* n. 616563, by the Italian Ministry of Education, University and Research (MIUR) through the "Dipartimenti di Eccellenza Program 2018-22 - Dept. of Mathematics, University of Pavia," and by the Istituto Nazionale di Alta Matematica (INdAM - GNCS), Italy.

Declarations

Conflict of interest The authors declare no competing interests.

References

1. Auricchio, F., Beirão da Veiga, L., Hughes, T.J.R., Reali, A., Sangalli, G.: Isogeometric collocation methods. Math. Mod. Meth. Appl. Sci. **20**(11), 2075–2107 (2010)
2. Auricchio, F., Beirão da Veiga, L., Hughes, T.J.R., Reali, A., Sangalli, G.: Isogeometric collocation for elastostatics and explicit dynamics. Comput. Meth. Appl. Mech. Eng. **249–252**, 2–14 (2012)
3. Bazilevs, Y., Beirão da Veiga, L., Cottrell, J.A., Hughes, T.J.R., Sangalli, G.: Isogeometric analysis: approximation, stability and error estimates for h-refined meshes. Math. Mod. Meth. Appl. Sci. **16**, 1–60 (2006)
4. Beirão da Veiga, L., Buffa, A., Sangalli, G., Vázquez, R.: Mathematical analysis of variational isogeometric methods. Acta Numer. **23**, 157–287 (2014)
5. Clayton, R., Engquist, B.: Absorbing boundary conditions for acoustic and elastic wave equations. Bull. Seism. Soc. Am. **67**(6), 1529–1540 (1977)
6. Cottrell, J.A., Hughes, T.J.R., Bazilevs, Y.: Isogeometric analysis. Wiley, Towards integration of CAD and FEA (2009)
7. Cottrell, J., Reali, A., Bazilevs, Y., Hughes, T.J.R.: Isogeometric analysis of structural vibrations. Comput. Methods Appl. Mech. Engrg. **195**, 5257–5296 (2006)
8. Dedé, L., Jaggli, C., Quarteroni, A.: Isogeometric numerical dispersion analysis for two-dimensional elastic wave propagation. Comput. Methods Appl. Mech. Engrg. **284**, 320–348 (2015)
9. De Falco, C., Reali, A., Vázquez, R.: GeoPDEs: a research tool for isogeometric analysis of PDEs. Adv. Eng. Softw. **42**(12), 1020–1034 (2011)
10. de Boor, C.: A practical guide to splines. Springer (2001)
11. Demko, S.: On the existence of interpolation projectors onto spline spaces. J. of Approx. Theory **43**, 151–156 (1985)
12. Engquist, B., Majda, A.: Radiation boundary conditions for acoustic and elastic wave equations. Commun. Pure Appl. Math. **32**, 313–357 (1979)
13. Evans, J.A., Hiemstra, R.R., Hughes, T.J.R., Reali, A.: Explicit higher-order accurate isogeometric collocation methods for structural dynamics. Comput. Methods Appl. Mech. Engrg. **338**(15), 208–240 (2018)
14. Gahalaut, K., Tomar, S.: Condition number estimates for matrices arising in the isogeometric discretization. Tech. Report 2012-23, RICAM (2012)

15. Garoni, C., Manni, C., Pelosi, F., Serra Capizzano, S., Speelers, H.: On the spectrum of stiffness matrices arising from isogeometric analysis. Numer. Math. **127**(4), 751–799 (2014)
16. Gervasio, P., Dedé, L., Chanon, O., Quarteroni, A.: A computational comparison between isogeometric analysis and spectral element methods: accuracy and spectral properties. J. Sci. Comp. **83**, 1–45 (2020)
17. Givoli, D.: Non-reflecting boundary conditions. J. Comput. Phys. **94**(1), 1–29 (1991)
18. Gomez, H., De Lorenzis, L.: The variational collocation method. Comput. Methods Appl. Mech. Engrg. **309**, 152–181 (2016)
19. Hughes, T.J.R., Cottrell, J.A., Bazilevs, Y.: Isogeometric analysis: CAD, finite elements, NURBS, exact geometry, and mesh refinement. Comp. Meth. Appl. Mech. Engrg. **194**, 4135–4195 (2005)
20. Hughes, T.J.R., Reali, A., Sangalli, G.: Isogeometric methods in structural dynamics and wave propagation. In: Papadrakakis, M. et al. (eds.) COMPDYN 2009 (2009)
21. Ihlenburg, F.: Finite element analysis of acoustic scattering. Applied Mathematical Sciences, 132. Springer-Verlag, Berlin, (1998)
22. Junger, M.C., Feit, D.: Sound. Structures and their interaction. MIT Press, Cambridge, MA (1986)
23. Komatitsch, D., Ritsema, J., Tromp, J.: Accurate solutions of wave propagation problems under impact loading by the standard, spectral and isogeometric high-order finite elements. Comparative study of accuracy of different space-discretization techniques. Finite Elem. Anal. Des. **88**, 67–89 (2014)
24. Loli, G., Sangalli, G., Tani, M.: Easy and efficient preconditioning of the isogeometric mass matrix. Comput. Math. Appl. **116**, 245–264 (2022)
25. Kruse, R., Nguyen-Thanh, N., De Lorenzis, L., Hughes, T.J.R.: Isogeometric collocation for large deformation elasticity and frictional contact problems. Comp. Meth. Appl. Mech. Engrg. **296**, 73–112 (2015)
26. Montardini, M., Sangalli, G., Tamellini, L.: Optimal-order isogeometric collocation at Galerkin superconvergent points. Comput. Methods Appl. Mech. Engrg. **316**, 741–757 (2017)
27. Mur, G.: Absorbing boundary conditions for the finite-difference approximation of the time-domain electromagnetic-field equations. IEEE Trans. Elect. Compat. **23**(4), 377–382 (1981)
28. Newmark, N.M.: A method of computation for structural dynamics. Proceedings of ASCE J. Eng. Mechanics (EM3) **85**, 67–94 (1959)
29. Quarteroni, A., Tagliani, A., Zampieri, E.: Generalized Galerkin approximations of elastic waves with absorbing boundary conditions. Comput. Methods Appl. Mech. Engrg. **163**, 323–341 (1998)
30. Rogers, D.F.: An introduction to NURBS with historical perspective. Academic Press, (2001)
31. Schumaker, L.L.: Spline functions: basic theory, 3rd edn. Cambridge University Press, Cambridge, Cambridge Mathematical Library (2007)
32. Schillinger, D., Evans, J.A., Reali, A., Scott, M.A., Hughes, T.J.R.: Isogeometric Collocation: cost comparison with Galerkin methods and extension to adaptive hierarchical NURBS discretizations. Comp. Meth. Appl. Mech. Engrg. **267**, 170–232 (2013)
33. Vázquez, R.: A new design for the implementation of isogeometric analysis in Octave and Matlab: GeoPDEs 3.0. IMATI REPORT Series 16-02, (2016)
34. Wood, W.L.: A further look at Newmark Houbolt, etc., time-stepping formulae. Int. J. Numer. Meth. Engrg. **20**, 1009–1017 (1984)
35. Wood, W.L.: Practical time-stepping schemes. Clarendon Press, Oxford (1990)
36. Zampieri, E., Pavarino, L.F.: Explicit second order isogeometric discretizations for acoustic wave problems. Comput. Methods Appl. Mech. Engrg. **348**, 776–795 (2019)
37. Zampieri, E., Pavarino, L.F.: Isogeometric collocation discretizations for acoustic wave problems. Comput. Methods Appl. Mech. Engrg. **385**, 114047 (2021)
38. Zhu, S., Dedé, L., Quarteroni, A.: Isogeometric analysis and proper orthogonal decomposition for the acoustic wave equation. ESAIM: Math. Meth. Numer. Anal. **51**, 1197–1221 (2017)